Phytochemistry 236 (2025) 114490

Contents lists available at ScienceDirect

Phytochemistry

journal homepage: www.elsevier.com/locate/phytochem

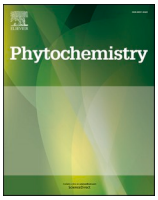

Indole alkaloids from *Uncaria rhynchophylla* and their inhibitory activities against α-glucosidase

Kepu Huang [a,b], Xuelin Chen [c], Sheng Li [a], Xinjian Zhang [a], Yumei Zhang [c,*], Yu Zhang [a,**]

[a] State Key Laboratory of Phytochemistry and Natural Medicines, Kunming Institute of Botany, Chinese Academy of Sciences, Kunming, 650201, China
[b] School of Pharmaceutical Science & Yunnan Key Laboratory of Pharmacology for Natural Products, Kunming Medical University, Kunming, 650500, China
[c] Key Laboratory of Tropical Plant Resource and Sustainable Use, Xishuangbanna Tropical Botanical Garden, Chinese Academy of Sciences, Kunming, 650223, China

ARTICLE INFO

Keywords:
Uncaria rhynchophylla
Rubiaceae
Uncarialines F-L
Quaternary ammonium alkaloid
α-Glucosidase

ABSTRACT

Sixteen indole alkaloids were isolated from the hook-bearing stems of *Uncaria rhynchophylla* (Rubiaceae family), including seven undescribed ones, uncarialines F-L (**1**–**5**, **7**, and **8**), and a naturally occurring alkaloid, 3-epicorynanthine (**6**). Among them, alkaloids **1** and **2** were identified as rare quaternary ammonium alkaloids, and alkaloid **7** exhibited an unprecedented indole alkaloid framework. Their structures were characterized by a comprehensive analysis of NMR, MS, ECD and single-crystal X-ray diffraction. Notably, alkaloid **5** demonstrate potent inhibitory activity against α-glucosidase, with an IC_{50} value of 18.45 $\pm$ 0.77 μM. Furthermore, the inhibitory kinetics of α-glucosidase revealed that alkaloid **5** belong to the mix inhibition type. Molecular docking analysis showed that alkaloid **5** possessed superior binding affinity with α-glucosidase (−10.7 kcal/mol).

1. Introduction

Diabetes mellitus (DM), a metabolic disorder characterized by persistent hyperglycemia, is prevalent globally (Ong et al., 2023). As the disease progresses, chronic hyperglycemia can lead to various complications, such as cardiovascular disease, nephropathy, neurological disorders, and retinopathy (Dong et al., 2024). α-glucosidase is a key enzyme in carbohydrate digestion. It is targeted by inhibitors that competitively bind to enzyme sites on the brush border membrane of the small intestine, thus modulating postprandial blood glucose levels (Gul et al., 2024). Hence, inhibiting α-glucosidase activity (Khan et al., 2024; S.K. Liu et al., 2021a; Xu et al., 2020) is one of the essential strategies for managing DM. Clinically, α-glucosidase inhibitors like acarbose and miglitol are utilized to treat DM. However, their high cost and side effects have limited their applications. Prior phytochemical studies have identified numerous plant-derived alkaloids as potential active substances that can reduce α-glucosidase activity (Hou et al., 2021; Li et al., 2020; Liu et al., 2021b; Teerapongpisan et al., 2024), offering an alternative approach.

Uncaria rhynchophylla (Miq.) Miq. ex Havil. (Rubiaceae family), known as “Gou Teng” in Chinese, is a renowned Traditional Chinese Medicine (TCM) used for treating cardiovascular and diabetes (Qin et al., 2021). To date, over 200 constituents, including alkaloids, triterpenoids, flavonoids, and phenylpropanoids, have been identified from the genus *Uncaria*, with alkaloids being the primary bioactive components responsible for the therapeutic effects of *U. rhynchophylla* (Qin et al., 2021). To further discover hypoglycemic indole alkaloids and explore the anti-diabetes constituents of *U. rhynchophylla*, seven undescribed indole alkaloids, uncarialines F-L (**1**–**5**, **7**, and **8**), along with a naturally existing alkaloid, 3-epicorynanthine (**6**), were obtained from *U. rhynchophylla*. Herein, we present their isolation, identification and inhibitory activities against α-glucosidase.

2. Results and discussion

Compound **1** was obtained as white solid. It had a molecular formula of $C_{23}H_{31}N_2O_4^+$ in terms of HRESIMS ion at *m/z* 399.2286 ($[M]^+$, calcd for 399.2278). ^{13}C and DEPT NMR spectrum revealed **1** possessed 23 carbon signals including six sp^2 quaternary carbons, six sp^3 methylenes, five sp^2 methines, three sp^3 methines, two methoxys, and one methyl moieties. Detailed analysis demonstrated that **1** had structural similarities with that of corynantheidine (Wenkert et al., 1973), with exception of a distinct hydroxymethyl signal [δ_H 5.25 (1H, d, CH_2-23), 5.72 (1H, d, CH_2-23); δ_C 83.1 (C-23)]. The key HMBC correlations of CH_2-23 (δ_H

* Corresponding author.
** Corresponding author.
E-mail addresses: zymei@xtbg.ac.cn (Y. Zhang), zhangyu@mail.kib.ac.cn (Y. Zhang).

https://doi.org/10.1016/j.phytochem.2025.114490
Received 21 November 2024; Received in revised form 18 March 2025; Accepted 22 March 2025
Available online 25 March 2025

5.25) to C-3 (δ_C 59.4), C-5 (δ_C 57.6) and C-21 (δ_C 54.4) assigned the hydroxymethyl was linked with C-3, C-5, and C-21 via *N* atom, which formed a quaternary ammonium. Further 2D NMR experiments (HSQC, HMBC, ^{1}H–^{1}H COSY) finally confirmed the planar structure of **1** (Fig. 1). Additionally, the ROESY correlations between H-3 and H-15/H-20/CH_2-23 indicated that these protons were located on the same side. Meanwhile, the unobserved ROESY correlation of H-17 with CH_2-14 indicated an (*E*)-configuration of the $\Delta^{16(17)}$ double bond (Fig. 3). The absolute stereochemistry of (3*R*,15*R*,20*R*)-**1** was assigned finally by the compatible calculated and experimental ECD spectra of uncarialine F (**1**) (Fig. 4).

Compound **2** was obtained as white solid with the molecular formula $C_{23}H_{29}N_2O_4^+$, established by HRESIMS analysis (found: *m/z* 397.2130 $[M]^+$, calcd for 397.2122). The NMR data revealed that **2** shares the same basic scaffold as **1** (Tables 1 and 2). A striking difference was the presence of a vinyl group (δ_H 5.01, 5.06, δ_C 119.8; δ_H 5.11, δ_C 134.5) in **2**. The molecular weight of **2** has two less mass units and one more unsaturation than that of **1**, demonstrating **2** was the $\Delta^{18(19)}$ double bond oxidized form of **1**. The planar structure of **2** was thereby established (Fig. 1), which was verified by HMBC correlations of H-15 (δ_H 2.53) and CH_2-21 (δ_H 3.23) to C-19 (δ_C 134.5) and subsequent ^{1}H–^{1}H COSY analysis (Fig. 2). The identical ROESY and ECD spectra of **2** and **1** demonstrated both alkaloids possessed the same relative and absolute configurations (Figs. 3 and 4).

Compound **3** was obtained as pale-yellow solid. It had a molecular formula of $C_{22}H_{26}N_2O_4$, as given by HRESIMS analysis (found: *m/z* 383.1973 $[M+H]^+$, calcd for 383.1965). The IR absorptions implied the presence of amino or hydroxyl group (3427 cm^{-1}) and ester carbonyl (1700 cm^{-1}). Interpretation of its NMR data suggested **3** had a similarity with *Z*-geissoschizine methyl ether (Lounasmaa and Hanhinen, 1999), with the exception that the chemical shift value of C-10 was deshielded from δ_C 119.4 in *Z*-geissoschizine methyl ether to δ_C 151.2 in **3**. Moreover, the ^{1}H NMR spectrum showed three aromatic protons with an ABX coupling pattern: [δ_H 6.80 (1H, d, H-9), 6.63 (1H, dd, H-11), 7.10 (1H, d, H-12)], which indicated the presence of a hydroxyl group attached to C-10. This was further verified by the key HMBC correlations of H-12 to C-10 (δ_C 151.2) and H-9 to C-11 (δ_C 111.8). Thus, the planar structure of **3** was thereby established (Fig. 1). The ROESY correlation of CH_3-18 with H-15 and the unobserved ROESY correlation of H-17 with CH_2-14 confirmed the $\Delta^{19(20)}$ and $\Delta^{16(17)}$ double bonds took (*E*)- and (*E*)-configurations, respectively. Additionally, the unobserved ROESY correlation of H-3 with H-15 indicated that the H-3 and H-15 were opposite. Thus, there are two possible stereoisomers (3*S**,15*R**)-**3** or (3*R**,15*S**)-**3**. The absolute stereochemistry of (3*S*,15*R*)-**3** was assigned finally by the compatible calculated and experimental ECD spectra of uncarialine H (**3**) (Fig. 4).

Compound **4** was obtained as white solid. Its molecular formula, $C_{22}H_{28}N_2O_4$, was established by HRESIMS analysis (found: *m/z* 385.2126 $[M+H]^+$, calcd for 385.2122). IR absorptions showed the existence of amino or hydroxyl group (3425 cm^{-1}) and ester carbonyl (1697 cm^{-1}). The ^{1}H and ^{13}C NMR spectra of **4** closely resembled those of corynantheidine (Wenkert et al., 1973). A striking difference was the presence of a unique oxygen-linked methylene signal [δ_H 3.56 (2H, m, CH_2-18); δ_C 60.5 (C-18)] in **4**, which was further verified by the key ^{1}H–^{1}H COSY cross-peaks of CH_2-18/CH_2-19/H-20 and the HMBC correlation of CH_2-18 (δ_H 3.56) to C-20 (δ_C 34.0). Thus, alkaloid **4** was established as 18-hydroxyl form of corynantheidine. The opposite configurations of H-3 and H-15 were established by the invisible ROESY correlation of H-3 and H-15. Moreover, the ROESY correlation of H-15 with CH_2-19 and the invisible ROESY correlation of H-17 with CH_2-14 indicated *β*-orientation of H-15, *α*-orientation of H-20 and an (*E*)-configuration of the $\Delta^{16(17)}$ double bond, respectively. The absolute stereochemistry of (3*S*,15*R*,20*S*)-**4** was assigned finally by ECD calculation at B3LYP/6-31G (d, p) level, as shown in Fig. 4.

Compound **5** was obtained as pale-yellow solid with a molecular formula of $C_{27}H_{34}N_2O_{10}$ according to positive HRESIMS data (m/z

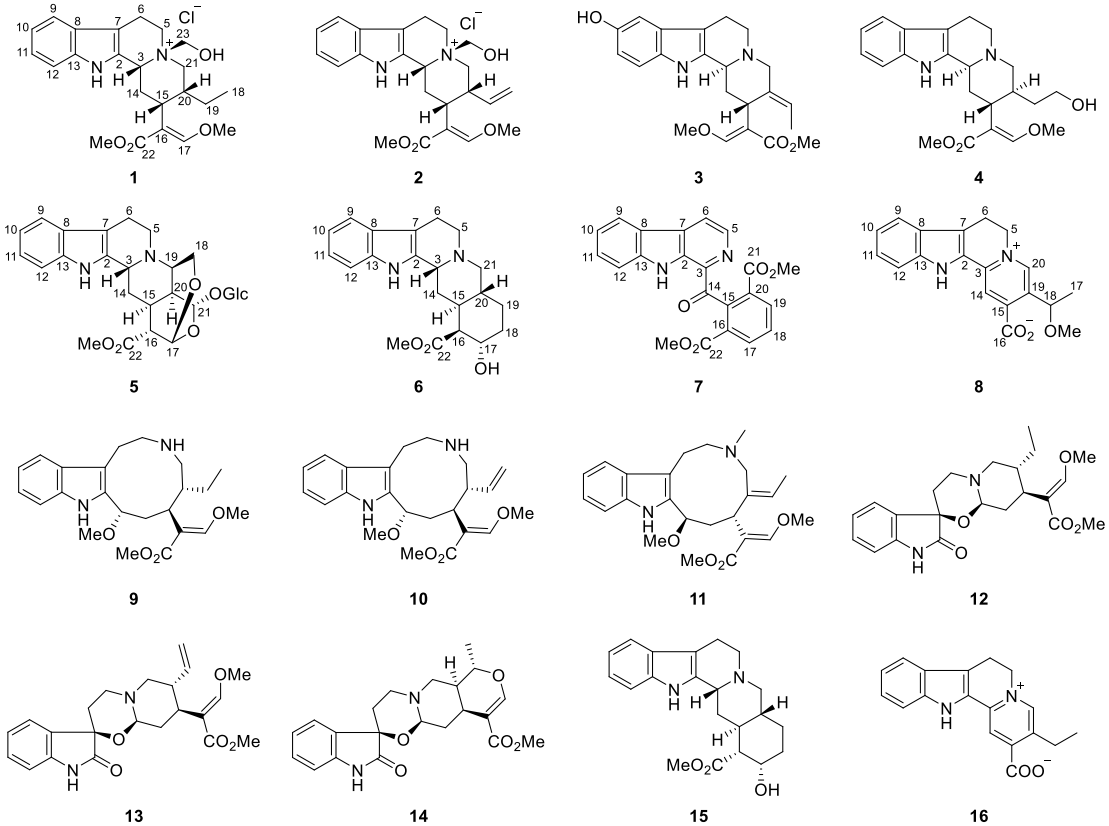

Fig. 1. Molecular structures of compounds **1**–**16**.

Table 1
^{1}H NMR spectroscopic data for compounds **1–8** (500 MHz, δ in ppm, J in Hz).

NO.	1[a]	2[a]	3[b]	4[a]	5[b]	6[b]	7[b]	8[b]
3	5.11 (s)	5.18 (br s)	3.73 (s)	4.65 (br s)	4.29 (d, 11.0)	4.46 (s)		
5a	3.69 (m)	3.76 (m)	2.81 (m)	3.37 (td, 14.5, 5.5)	2.90 (dd, 13.0, 4.0)	3.22 (m)	8.22 (d, 5.0)	4.87 (t, 7.0)
5b	3.69 (m)	3.76 (m)	3.10 (dt, 10.5, 5.0)	3.44 (td, 14.5, 7.0)	3.05 (m)	3.22 (m)		4.87 (t, 7.0)
6a	2.76 (m)	2.90 (br s)	2.72 (dt, 15.0, 4.0)	2.75 (dd, 16.0, 5.5)	2.74 (m)	2.58 (m)	8.26 (d, 5.0)	3.41 (t, 7.0)
6b	2.95 (m)	2.98 (m)	2.89 (m)	3.04 (m)	2.89 (m)	3.04 (m)		3.41 (t, 7.0)
9	7.39 (d, 8.0)	7.43 (d, 8.0)	6.80 (d, 2.0)	7.50 (d, 8.0)	7.37 (d, 8.0)	7.39 (d, 8.0)	8.27 (d, 8.0)	7.66 (d, 8.0)
10	7.12 (t, 8.0)	7.14 (t, 8.0)		7.14 (t, 8.0)	6.96 (t, 8.0)	6.98 (td, 8.0, 1.0)	7.35 (td, 8.0, 1.0)	7.17 (td, 8.0, 1.0)
11	7.22 (t, 8.0)	7.23 (t, 8.0)	6.63 (dd, 8.5, 2.0)	7.20 (t, 8.0)	7.03 (t, 8.0)	7.06 (td, 8.0, 1.0)	7.64 (td, 8.0, 1.0)	7.36 (td, 8.0, 1.0)
12	7.45 (d, 8.0)	7.45 (d, 8.0)	7.10 (d, 8.5)	7.42 (d, 8.0)	7.26 (d, 8.0)	7.30 (d, 8.0)	7.78 (d, 8.0)	7.47 (d, 8.0)
14a	2.30 (d, 12.0)	2.35 (d, 16.0)	2.08 (ddd, 12.5, 5.0, 2.5)	2.11 (d, 14.0)	1.82 (td, 14.0, 5.0)	1.54 (dt, 14.0, 4.0)		7.98 (s)
14b	2.98 (m)	3.01 (m)	2.34 (q, 12.5)	2.61 (m)	2.17 (d, 14.0)	2.15 (m)		
15	2.37 (td, 12.0, 4.0)	2.53 (td, 13.0, 4.0)	3.80 (m)	2.32 (t, 10.0)	3.17 (m)	1.69 (d, 13.0)		
16					2.91 (m)	2.44 (dd, 11.0, 5.0)		
17	7.36 (s)	7.33 (s)	7.44 (s)	7.35 (s)	5.66[c]	4.03 (td, 11.0, 5.0)	8.32 (d, 8.0)	1.51 (d, 6.5)
18a	0.71 (t, 7.5)	5.01 (td, 10.0, 2.0)	1.57 (d, 7.0)	3.56 (m)	3.74 (dd, 14.0, 4.0)	1.31 (m)	7.75 (t, 8.0)	4.95 (q, 6.5)
18b		5.06 (br s)		3.56 (m)	4.23 (d, 14.0)	2.06 (m)		
19a	0.80 (br s)	5.11 (q, 10.0)	5.47 (q, 7.0)	1.04 (ddt, 14.0, 9.0, 6.0)	3.26 (m)	2.01[c]	8.32 (d, 8.0)	
19b	1.34 (br s)			1.54 (dt, 14.0, 6.0)		2.01[c]		
20	2.55 (m)	3.38 (m)		2.60 (m)	2.63 (t, 6.0)	2.01[c]		8.66 (s)
21a	3.07 (t, 13.0)	3.23 (m)	3.30 (d, 12.5)	2.59 (m)	5.66[c]	2.58 (d, 12.0)		
21b	3.32 (d, 13.0)	3.23 (m)	3.59 (d, 12.5)	3.09(m)		3.12 (dd, 12.0, 4.0)		
23a	5.25 (d, 8.0)	5.31 (d, 9.0)						
23b	5.72 (d, 8.0)	5.71 (d, 9.0)						
17-OMe	3.82 (s)	3.82 (s)	3.87 (s)	3.79 (s)				
18-OMe								3.39 (s)
21-OMe							3.59 (s)	
22-OMe	3.65 (s)	3.64 (s)	3.70 (s)	3.69 (s)	3.78 (s)	3.83 (s)	3.59 (s)	
21-*O*-Glc								
1′					4.60 (d, 8.0)			
2′					3.20 (t, 8.0)			
3′					3.39 (t, 8.0)			
4′					3.27 (m)			
5′					3.29 (m)			
6′a					3.64 (dd, 12.0, 6.0)			
6′b					3.88 (dd, 12.0, 2.0)			

[a] Measured in $CDCl_3$.
[b] Measured in CD_3OD.
[c] Overlapped.

547.2293 [M + H]$^+$). ^{13}C NMR and DEPT spectra of **5** revealed the presence of 27 carbon atoms, six of which were assigned to a sugar unit (Table 2). Moreover, the ^{1}H NMR spectrum showed the presence of the anomeric proton signal of *β-D*-glucoside at δ_H 4.60 (1H, d, J = 8.0 Hz, H-1′). The NMR data of **5** were very similar to those of dehydraisodihydrocadambine (Liu et al., 2013a), with a distinct methoxyl group in **5** [δ_H 3.78 (3H, s); δ_C 53.1]. The HMBC correlation of H-21 (δ_H 5.66) to C-17 (δ_C 96.1), in combination with the downshift of C-17 (δ_C 96.1) and C-21 (δ_C 95.8), revealed that C-21 was connected to C-17 through an oxygen atom. The HMBC correlation of H-17 (δ_H 5.66) to C-18 (δ_C 59.6) indicated the connection of C-17 and C-18 via an oxygen atom to form a sevenmember ring. Meanwhile, HMBC correlation from H-1' (δ_H 4.60) to C-21 (δ_C 95.8) implied that the *β-D*-glucoside was linked to C-21. The planar structure of **5** was thereby established as shown in Fig. 1. The ROESY cross-peaks of H-16 with H-3/CH_2-18b established H-3 and H-16 took *β*-orientations while H-19 was *α*-oriented. Meanwhile, H-15 and H-20 were classified as *α*-orientations by the ROESY correlations of CH_2-14b with H-3/H-16 and of CH_2-14a with H-20. Additionally, H-17 and H-21 were classified as *α*- and *β*-orientation, respectively, due to the tension of the cage ring skeleton. The absolute configuration of **5** was finally established by ECD calculation at B3LYP/6-31G (d, p) level. Accordingly, the structure of **5** was elucidated as shown in Fig. 1.

Compound **6** was obtained as pale-yellow solid with a molecular formula of $C_{21}H_{26}N_2O_3$, confirmed by the positive ion peak in the HRESIMS (*m/z* 355.2013 [M + H]$^+$, calcd for 355.2016), indicating 10 degrees of unsaturation. It was identified as a yohimbine-type alkaloid on the basis of peaks in the 1D NMR at δ_H 2.44 (1H, dd, H-16), 4.03 (1H, td, H-17), 1.31 (1H, m, CH_2-18), 2.06 (1H, m, CH_2-18), 2.01 (2H, CH_2-19), and δ_C 55.9 (C-16), 66.9 (C-17), 35.4 (C-18), 25.2 (C-19), together with the presence of an intense band at 282 nm in the UV spectrum. Meanwhile, its NMR data indicated that **6** had the same planar structure with 3-epicorynanthine (Janot et al., 1961), which was further verified by the ^{1}H–^{1}H COSY cross-peaks of H-3/CH_2-14/H-15/H-16/H-17/CH_2-18/CH_2-19/H-20/CH_2-21 and the HMBC correlations of H-15 and 22-OMe to C-22. The relative configuration of **6** was established by ROESY correlations of CH_2-18a with H-15/H-16, H-20 with H-3/H-17,

Table 2
^{13}C NMR spectroscopic data for compounds **1–8** (125 MHz, δ in ppm).

No	1[a]	2[a]	3[b]	4[a]	5[b]	6[b]	7[b]	8[b]
2	126.1	125.9	135.8	130.7	136.4	132.2	135.9	125.9
3	59.4	59.6	59.8	54.5	51.2	55.6	139.0	143.8
5	57.6	57.6	52.2	51.0	50.6	52.3	138.2	57.1
6	16.4	16.4	22.0	16.7	22.7	17.4	119.4	20.4
7	104.7	104.8	107.3	107.2	108.1	107.7	133.2	118.5
8	125.7	125.7	128.8	127.3	128.3	128.7	121.8	126.0
9	118.0	118.1	103.3	118.1	118.5	118.6	122.7	121.1
10	120.1	120.2	151.2	119.8	119.7	119.9	121.6	122.1
11	123.1	123.3	111.8	122.0	121.9	122.2	130.3	127.6
12	112.6	112.7	112.4	111.4	111.8	112.1	113.6	113.4
13	137.2	137.2	132.9	136.2	138.2	137.9	143.6	141.2
14	26.2	26.0	34.0	31.1	36.6	24.9	199.5	118.5
15	32.6	31.2	37.1	34.0[c]	23.9	37.0	145.3	156.6
16	108.9	108.3	113.2	110.6	52.3	55.9	131.5	170.3
17	160.8	161.2	161.4	160.3	96.1	66.9	135.3	23.1
18	10.6	119.8	13.6	60.5	59.6	35.4	130.4	75.5
19	24.2	134.5	123.1	34.2	62.4	25.2	135.3	137.8
20	32.6	36.5	134.9	34.0[c]	40.0	33.9	131.5	143.9
21	54.4	53.5	64.7	51.0	95.8	50.7	167.2	
22	168.1	168.2	170.1	168.7	174.8	175.3	167.2	
23	83.1	83.2						
17-OMe	61.5	62.2	62.4	61.8				
18-OMe								57.5
21-OMe							52.9	
22-OMe	50.9	51.5	52.0	51.5	53.1	52.2	52.9	
21-*O*-Glc								
1′					99.6			
2′					74.9			
3′					77.7			
4′					71.6			
5′					78.3			
6′					62.8			

[a] Measured in $CDCl_3$.
[b] Measured in CD_3OD.
[c] Overlapped.

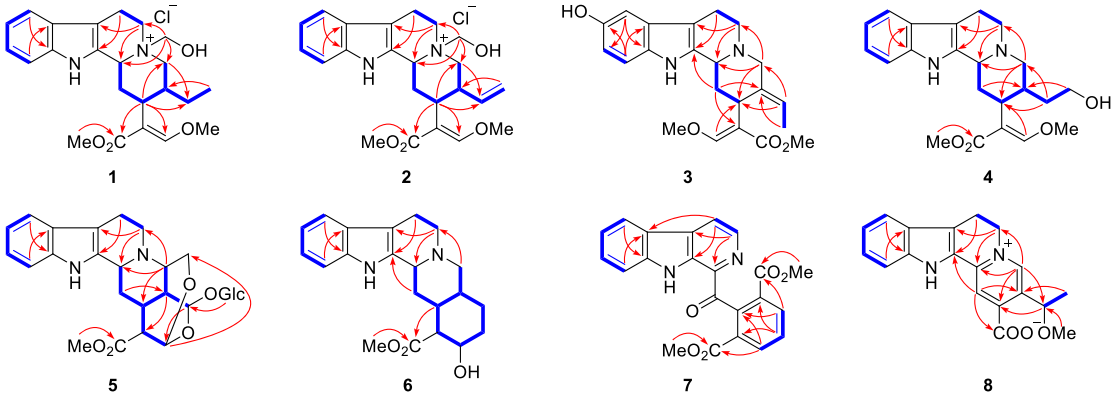

Fig. 2. Key HMBC (arrow) and ^{1}H–^{1}H COSY (bold) correlations of compounds **1**–**8**.

as shown in Fig. 3. The absolute stereochemistry of (3*R*,15*S*,16*S*,17*S*,20*R*)-**6** was finally assigned by the compatible calculated and experimental ECD spectra of **6**. Therefore, compound **6** was established as 3-epicorynanthine, a stereoisomer of yohimbine obtaining via chemical transformation (Janot et al., 1961). As a naturally occurring alkaloid, the absolute configuration and NMR characteristics of compound **6** were reported here for the first time.

Compound **7** was obtained as pale-yellow crystals. The molecular formula, $C_{22}H_{16}N_2O_5$, was determined based on the presence of a *pseudo*-molecular ion peak at *m/z* 389.1134 ($[M + H]^+$) in the HRESIMS. NMR spectral data (Tables 1 and 2) demonstrated the existence of a β-carboline system (δ_C 135.9, 139.0, 138.2, 119.4, 133.2, 121.8, 122.7, 121.6, 130.3, 113.6, 143.6), a trisubstituted aromatic ring [δ_H 8.32 (2H, d, J = 8.0 Hz, H-17/19), 7.75 (1H, t, J = 8.0 Hz, H-18)], two methyl carboxylate moieties [(δ_H 3.59 (6H, s, OMe); δ_C 52.9 (OMe)], and a carbonyl group (δ_C 199.5). Key HMBC correlations of H-17/22-OMe to C-22, and of H-19/21-OMe to C-21, revealed the connections of two methyl carboxylate moieties to C-16 and C-20, respectively. Meanwhile, since the β-carboline system and the trisubstituted benzene ring moiety account for all the protons, they might be connected via the carbonyl group (C-14) between C-3 and C-15 positions. The structure of compound **7** was finally established through X-ray diffraction data analysis using Cu Kα radiation, with a Flack parameter of 0.20(10) (CCDC 2395497, Fig. 5).

Compound **8** was obtained as yellow crystals. Its HRESIMS data (*m/z* 345.1203 $[M + Na]^+$, calcd for 345.1210) established a molecular formula of $C_{19}H_{18}N_2O_3$, indicating 12 degrees of unsaturation. The IR spectrum showed absorption bands at 3432 and 1616 cm^{-1}, revealing

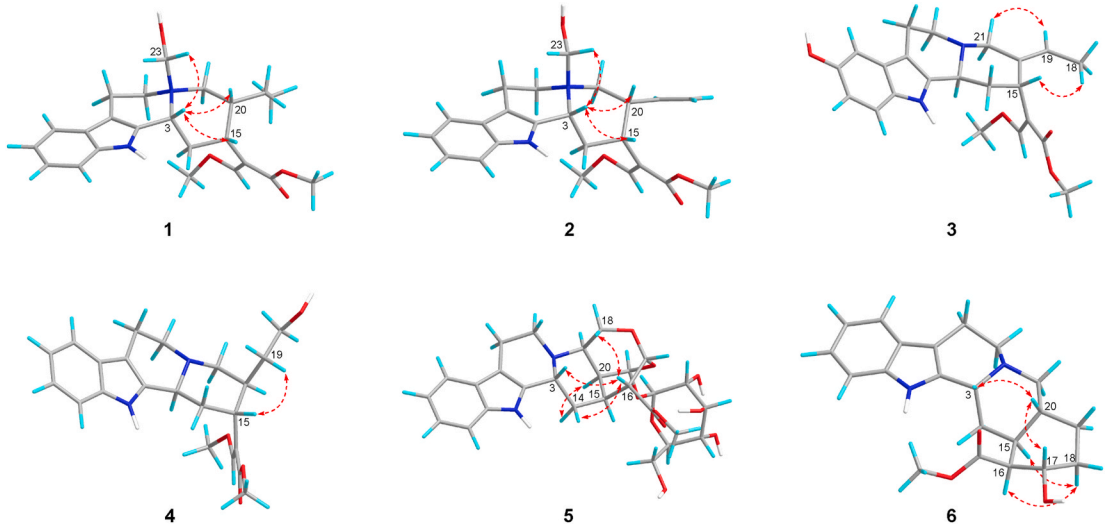

Fig. 3. Key ROESY correlations of compounds **1**–**6**.

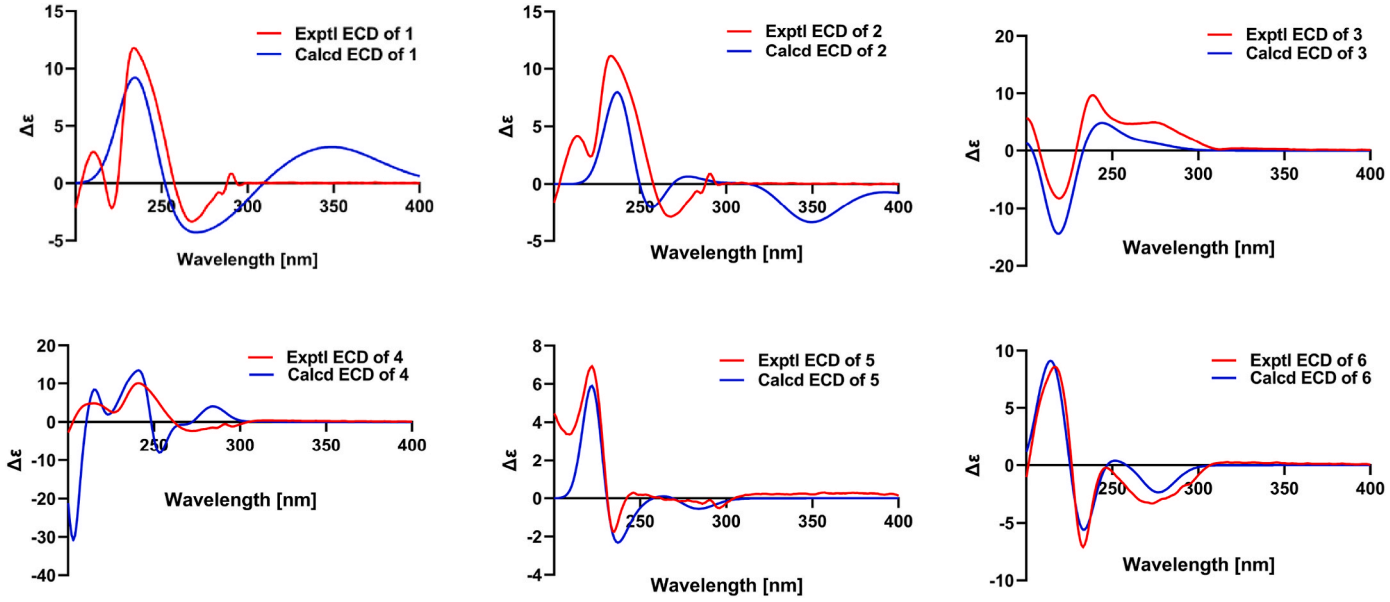

Fig. 4. Calculated and experimental ECD of compounds **1**–**6**.

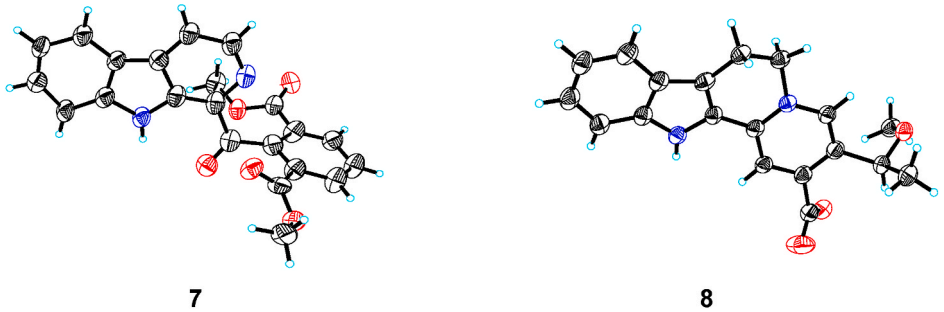

Fig. 5. Single-crystal X-ray structures of compounds **7** and **8** drawn with 30 % probability displacement ellipsoids.

the presence of an amino or hydroxyl group and a carboxylate anion, respectively. This finding coupled with its extreme insolubility in common organic solvents indicated the possibility of a zwitterionic structure. The aromatic region of the ^{1}H-NMR spectrum of **8** showed the presence of two sets of aromatic protons (Table 1). Two sets corresponding to an indole moiety at δ_H 7.66 (1H, d, J = 8.0 Hz, H-9), 7.17 (1H, td, J = 8.0, 1.0 Hz, H-10), 7.36 (1H, td, J = 8.0, 1.0 Hz, H-11), 7.47 (1H, d, J = 8.0 Hz, H-12), as well as a tetrasubstituted aromatic ring with

two isolated protons at δ_H 7.98 (s, H-14) and 8.66 (s, H-20), respectively. Resonances from the coupling systems at δ_H 4.87 (2H, t, $J = 7.0$ Hz, CH_2-5) with δ_H 3.41 (2H, t, $J = 7.0$ Hz, CH_2-6), and δ_H 1.51 (3H, d, $J = 6.5$ Hz, CH_3-17) with δ_H 4.95 (1H, q, $J = 6.5$ Hz, H-18) suggested the presence of a $–CH_2(N^+)–CH_2–$C-unit and an ethyl group. These were confirmed by the $^1H–^1H$ COSY cross-peaks of CH_2-5/CH_2-6, and CH_3-17/H-18, respectively. NMR spectral data (Tables 1 and 2) indicated the existence of a methoxy group at [δ_H 3.39 (3H, s, 18-OMe); δ_C 57.6 (18-OMe)], as well as a carboxylate anion at δ_C 170.3 (C-16). The key HMBC correlation of 18-OMe to C-18 implied the methoxy group was attached to C-18. The assignment of a carboxylate anion attached to C-15 was verified by HMBC correlation of H-14 to C-16. Thus, the planar structure of **8** was thereby established (Fig. 1). Meanwhile, hardly detected specific rotation indicated that **8** was a racemic combination, which was verified by the single-crystal X-ray diffraction (CCDC 2395498) (Fig. 5). Regrettably, the chiral separation of **8** was not achieved since the amount of racemate was insufficient.

In addition, the other eight known indole alkaloids were identified as uncarialines A-E (Huang et al., 2023), uncarialin D (Liang et al., 2019), pseudoyohimbine (Kam et al., 1992) and dihydrovincarpine (Ali et al., 1976), respectively, by comparing the spectroscopic data with the reported literatures.

To find active compounds with α-glucosidase inhibitory activity, compounds **1**–**8** were screened for their α-glucosidase inhibitory activities, and the results were shown in Table 3. Compound **5** demonstrated the most potent α-glucosidase inhibitory activity with an IC_{50} value of 18.45 ± 0.77 μM (Fig. 6).

To clarify how and where compound **5** binds to α-glucosidase, the enzyme kinetics of compound **5** was measured. As shown in Fig. 7a, the plot of compound **5** intersected in the third quadrant, with the increasing of inhibitor concentrations, the V_{max} and K_m values were decreased, indicating that compound **5** was non-competitive and reverse-competitive mixed inhibition types. We also examined Dixon plot of how compound **5** affect α-glucosidase. As shown in Fig. 7b, this plot further confirmed that compound **5** was mixed-type α-glucosidase inhibitors. The K_i and K_i' values of compound **5** were 9.44 ± 2.38 and 5.14 ± 1.84 μM, respectively. The results showed that the K_i' value was smaller than the K_i value, which indicated that the inhibitor-enzyme-substrate complex binding affinity exceeds the binding affinity of the inhibitor-enzyme. The molecular docking of compound **5** with enzyme was performed to determine the binding sites and mechanism underlying inhibition. Interestingly, the glycan group in **5** interacts with the residues ASN443, ARG450, and GLN439 of α-glucosidase (PDB:3WY1) and forms three hydrogen bonds (see Fig. 8). Notably, the strongest hydrogen bonding was with residue ASN443 of α-glucosidase resulting in a binding energy of −10.7 kcal/mol, and the distance was 2.2 Å. Current evidence may indicate that compound **5** has potential inhibitory activity of α-glucosidase due to the presence of additional glycan group, compared to other analogs. In summary, the docking results indicated that compound **5** might bind to the active site of α-glucosidase to inhibit the activity of the enzyme.

Table 3
α-Glucosidase inhibitory activities of compounds **1–8**.

Compounds	Inhibitory Rate (%)	IC_{50} (μM)
1[a]	n.d.	>50
2[a]	n.d.	>50
3[a]	n.d.	>50
4[a]	n.d.	>50
5[a]	76.86 ± 0.10	18.45 ± 0.77
6[a]	n.d.	>50
7[a]	n.d.	>50
8[a]	7.00 ± 0.74	>50
Acarbose[b]	92.16 ± 0.27	0.002 ± 0.01

Data were expressed as the mean value ± SD (n = 3); n.d. not determined.
[a] percent inhibition at a concentration of 50 μM.
[b] percent inhibition at a concentration of 0.025 μM.

3. Conclusions

In this investigation, a total of sixteen indole alkaloids were isolated from the methanol extract of the hook-bearing stems of *U. rhynchophylla*, including seven undescribed ones, namely uncarialines F-L (**1**–**5**, **7**, and **8**), and a naturally occurring alkaloid, 3-epicorynanthine (**6**). Alkaloids **1** and **2** were identified as rare quaternary ammonium alkaloids, while alkaloid **8** was confirmed as a zwitterionic molecule. The inhibitory activity of alkaloids **1**–**8** against α-glucosidase was evaluated, and alkaloid **5** demonstrated significant inhibitory activity. The inhibitory kinetics of α-glucosidase revealed that **5** caused a mixed-type inhibition, indicating that it could bind to both the free enzyme and the enzyme-substrate complex. In addition, the molecular docking results showed that **5** may bind to the active site through a glycan group, suggesting that the indole glycoalkaloid may be potential candidate for the treatment of metabolic diseases such as diabetes.

4. Experimental

4.1. General experimental procedures

Melting points were obtained on an XRC-1 apparatus and are uncorrected. NMR spectra were recorded on Bruker AV-500 MHz with TMS as an internal standard. HRESIMS were surveyed on Aglient 1290 UPLC/6540 Q-TOF spectrometer. IR spectra were surveyed on a Bio-Rad FTS-135 with KBr pellets. A JASCO P-1020 digital polarimeter was used to get optical rotations, while the ECD spectral data were measured by an Applied Photophysics Chariscan Spectrometer. Silica gel (60–80, 100–200, 200–300 and 300–400 mesh, Qingdao Marine Chemical Inc., China), silica gel H (10–40 μm, Qingdao Marine Chemical Inc., China), and Sephadex LH-20 (40–70 μm, Amersham Pharmacia Biotech AB), were used for column chromatography. Semi-preparative HPLC was carried out using a Shimadzu LC-20AT liquid chromatograph equipped with a YMC Triart C18 ExRS (5 μm; 10 × 250 mm) reversed-phase column.

Phosphate buffered saline (PBS) were purchased from Biological Industries (Shanghai, China). Dimethyl sulfoxide (DMSO) was obtained from Solarbio (Beijing, China). α-Glucosidase, acarbose, and 4-nitrophenyl-α-D-glucopyranoside (*p*NPG) were purchased from Yuanye Biotech Co., Ltd. (Shanghai, China). The other chemicals and reagents were purchased from local suppliers. The absorbance was measured by a microplate reader (Molecular Devices, Palo Alto, Santa Clara, CA, USA).

4.2. Plant material

The hook-bearing stems of *Uncaria rhynchophylla* (Miq.) Miq. ex Havil. were collected in Jianhe, Guizhou Province, China, on May 20, 2020, and was identified by Prof. Shunlin Li, Kunming Institute of Botany. The sample specimen (No. H20200520) was deposited at Key Laboratory of Phytochemistry and Natural Medicines, Kunming Institute of Botany, Chinese Academy of Sciences (CAS).

4.3. Extraction and isolation

The dried stems of *U. rhynchophylla* (50 kg) were powdered and extracted three times with methanol. The pH of extract was adjusted to 2–3 with hydrochloric acid (5 %) and then extracted three times with petroleum ether and ethyl acetate. The water fraction was basified to pH 9–10 with sodium hydroxide (10 %), then extracted with chloroform to get the crude alkaloids. The crude alkaloids (2030.0 g) were separated on a silica gel column (100–200 mesh), and eluted with a gradient of dichloromethane (DCM)/MeOH (49:1 → 1:1, v/v) to yield six fractions (A-F). Among them, fraction B (18.0 g) was divided into three fractions (B_1–B_3) by a silica gel column (300–400 mesh, DCM/MeOH, 49:1, 29:1,

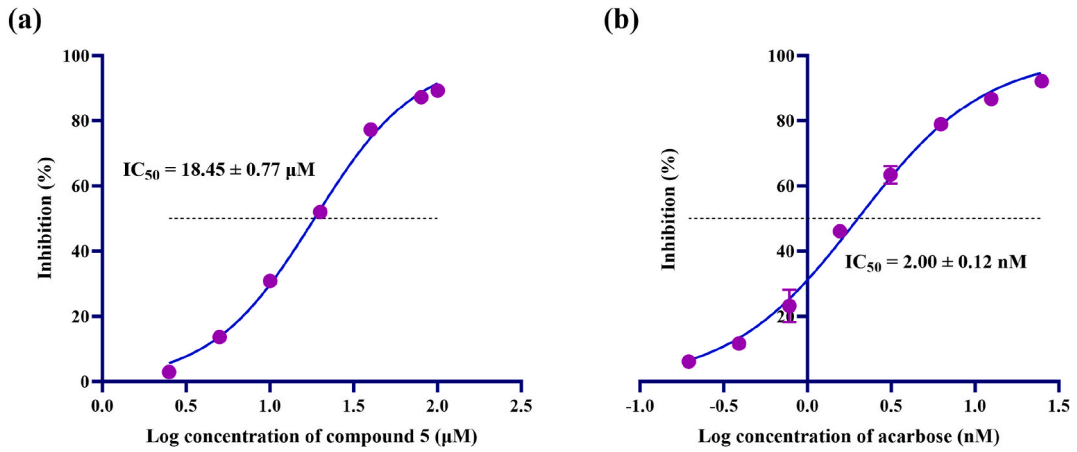

Fig. 6. α-Glucosidase inhibitory effects of compound **5**. (a) Log concentration-inhibition rate fitting curve of compound **5**. (b) Log concentration-inhibition rate fitting curve of acarbose. Calculated IC_{50} values of different groups by Statistical Product and Service Solutions (SPSS, version: 21.0), and all values are mean ± SD from a least three independent experiments.

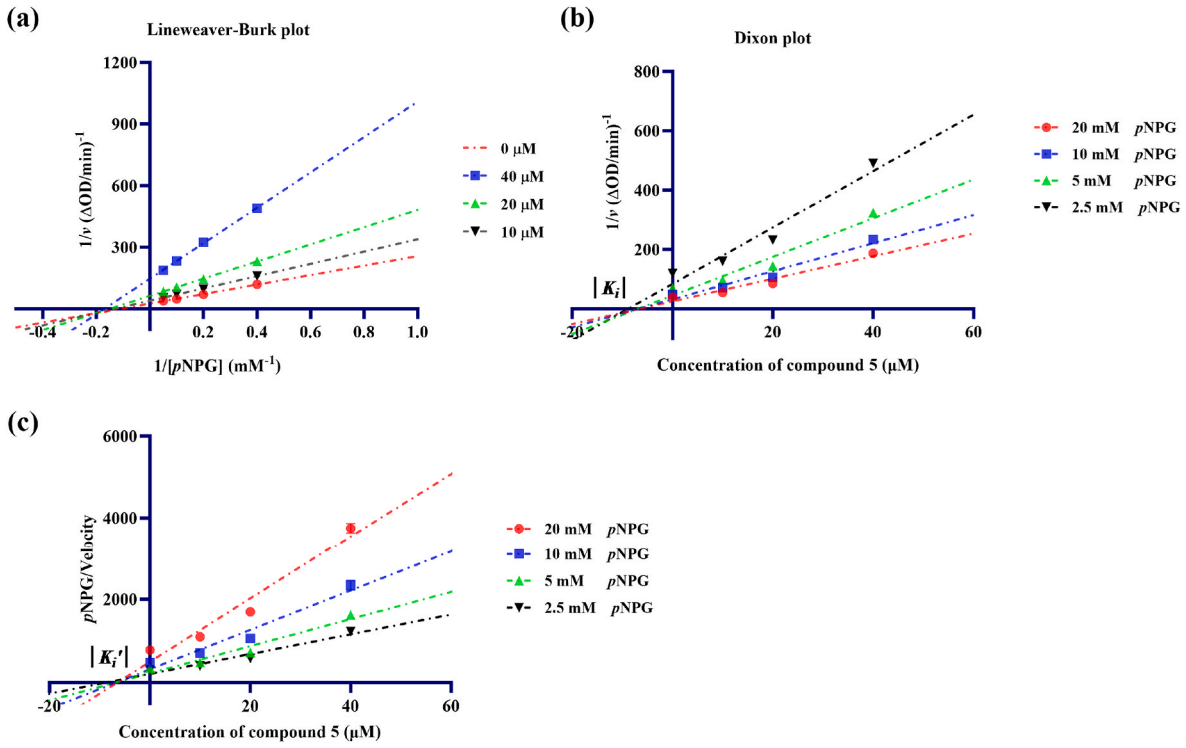

Fig. 7. Determination of K_i and K_i' of compound **5** on α-glucosidase. (a) 1/[*p*NPG]-1/*v* fitting curve of compound **5**. (b) 1/*v*-[I] fitting curve of compound **5**. (c) [*p*NPG]/*v*-[I] fitting curve of compound **5**. All values are mean ± SD from at least three independent experiments.

9:1, 1:1, v/v). Fraction B_2 (1.8 g) was separated by HPLC with MeCN/H_2O (60:40, 3 mL/min) to give **14** (13.0 mg, t_R 15.0 min). Fraction C (96.0 g) was divided to seven fractions (C_1–C_7) by a silica gel column (DCM/MeOH, 49:1, 19:1, 9:1, 1:1, v/v). Fraction C_3 (4.2 g) was separated by RP-C18 (MeOH/H_2O, 30:70, 50:50, 100:0, v/v) and HPLC with MeCN/H_2O (52:48, 3 mL/min) to give **12** (5.0 mg, t_R 11.0 min) and **13** (7.0 mg, t_R 28.0 min). Fraction E (184.0 g) was divided to nine fractions (E_1-E_9) by silica gel column chromatography (DCM/MeOH, 19:1, 9:1, 1:1, v/v). Fraction E_2 (520.0 mg) was separated by Sephadex LH-20 (MeOH) and HPLC with MeCN/H_2O (45:55, 3 mL/min) to obtain **10** (9.0 mg, t_R 9.0 min) and **9** (11.0 mg, t_R 18.0 min). Fraction E_3 (210 mg) was further separated by HPLC with MeCN/H_2O (37:63, 3 mL/min) to give **3** (6.0 mg, t_R 13.0 min), **4** (4.0 mg, t_R 20.5 min) and **7** (4.0 mg, t_R 23.5 min) Fraction E_5 (2.5 g) was separated by Sephadex LH-20 and subsequent HPLC separation with MeCN/H_2O (30:70, 3 mL/min) to obtain **11** (43.0 mg, t_R 38.0 min). Fraction F (104.0 g) was divided to five fractions (F_1–F_5) by silica gel column chromatography (DCM/MeOH, 14:1, 9:1, 1:1, v/v). Fraction F_2 (220.0 mg) was separated by Sephadex LH-20 (MeOH) and HPLC with MeOH/H_2O (40:60, 3 mL/min) to obtain **1** (6.0 mg, t_R 9.0 min) and **2** (4.0 mg, t_R 18.0 min). Fraction F_3 (1.2 g) was separated by Sephadex LH-20 (MeOH) and HPLC with MeOH/H_2O (38:62, 3 mL/min) to obtain **16** (4.0 mg, t_R 29.0 min) and **8** (5.0 mg, t_R 38.0 min). Fraction F_4 (12.0 g) was separated by Sephadex LH-20 (MeOH) and HPLC with MeOH/H_2O (36:64, 3 mL/min) to obtain **5** (5.0 mg, t_R 24.0 min). Fraction F_5 (25 g) was separated by RP-C18 (MeOH/H_2O, 20:80, 25:75, 100:0, v/v) to obtain **6** (6.0 mg) and **15** (9.0 mg).

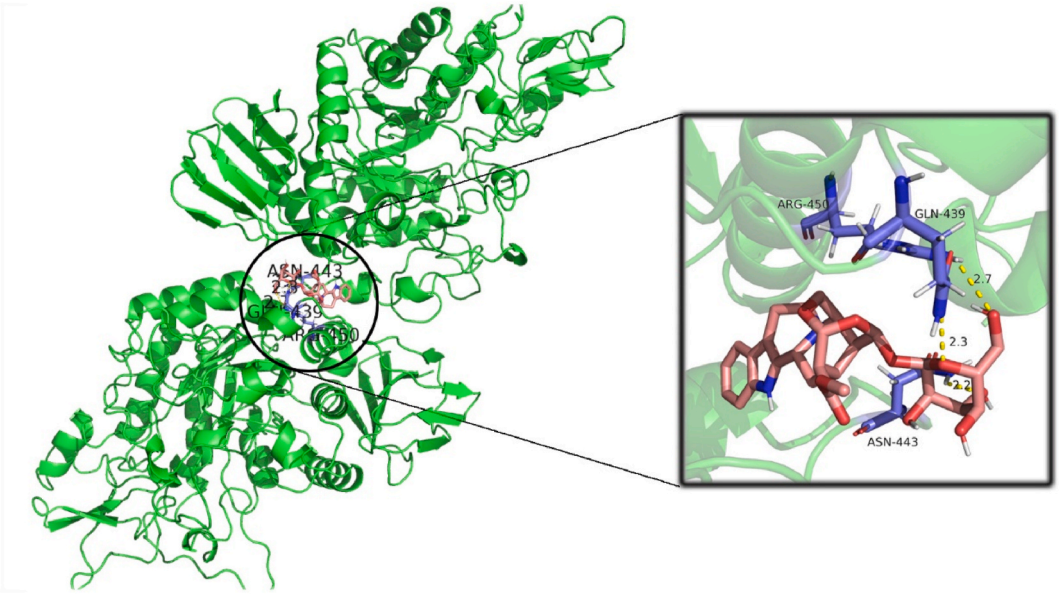

Fig. 8. Molecular docking result of compound **5** on α-glucosidase (PDB: 3WY1).

4.4. Compound characterization

Uncarialine F ***(1):*** white solid; [α] 57 (*c* 0.1, MeOH); UV (MeOH) λ_{max} (log ε): 220 (4.3) nm; ECD (0.0006 M, MeOH) λ_{max} ($\Delta\varepsilon$) 210 (+2.72), 234 (+11.70); IR (KBr) *v*max 3423, 2922, 2852, 1698, 1635, 1455, 1255, 1113 cm^{-1}; HRESIMS *m/z* 399.2286 $[M]^+$ (calcd for $C_{23}H_{31}N_2O_4^+$, 399.2278); ^1H and ^{13}C NMR data (CDCl3, 500 and 125 MHz) see Tables 1 and 2

Uncarialine G ***(2):*** white solid; [α] 46 (*c* 0.1, MeOH); UV (MeOH) λ_{max} (log ε): 220 (4.2) nm; ECD (0.0006 M, MeOH) λ_{max} ($\Delta\varepsilon$) 214 (+4.16), 234 (+11.12); IR (KBr) *v*max 3419, 2923, 2853, 1699, 1637, 1456, 1257, 1123 cm^{-1}; HRESIMS *m/z* 397.2130 $[M]^+$ (calcd for $C_{23}H_{29}N_2O_4^+$, 397.2122); ^1H and ^{13}C NMR data (CDCl3, 500 and 125 MHz) see Tables 1 and 2

Uncarialine H ***(3):*** pale-yellow solid; [α] 22 (*c* 0.06, MeOH); UV (MeOH) λ_{max} (log ε): 227 (4.2), 274 (3.7) nm; ECD (0.0005 M, MeOH) λ_{max} ($\Delta\varepsilon$) 219 (−8.27), 239 (+9.67); IR (KBr) *v*max 3427, 2940, 2851, 1700, 1634, 1439, 1247, 1148 cm^{-1}; HRESIMS *m/z* 383.1973 $[M+H]^+$ (calcd for $C_{22}H_{27}N_2O_4$, 383.1965); ^1H and ^{13}C NMR data (CD_3OD, 500 and 125 MHz) see Tables 1 and 2

Uncarialine I ***(4):*** white solid; [α] −1 (*c* 0.06, MeOH); UV (MeOH) λ_{max} (log ε): 224 (4.1) nm; ECD (0.0007 M, MeOH) λ_{max} ($\Delta\varepsilon$) 215 (+4.87), 241 (+10.08); IR (KBr) *v*max 3425, 2936, 2853, 1697, 1634, 1440, 1251, 1131 cm^{-1}; HRESIMS *m/z* 385.2126 $[M+H]^+$ (calcd for $C_{22}H_{29}N_2O_4$, 385.2122); ^1H and ^{13}C NMR data (CDCl3, 500 and 125 MHz) see Tables 1 and 2

Uncarialine J ***(5):*** pale-yellow solid; [α] 37 (*c* 0.1, MeOH); UV (MeOH) λ_{max} (log ε): 225 (4.6), 282 (3.9) nm; ECD (0.0002 M, MeOH) λ_{max} ($\Delta\varepsilon$) 222 (+6.93), 235 (−1.75); IR (KBr) *v*max 3431, 2924, 2853, 1723, 1628, 1439, 1070 cm^{-1}; HRESIMS *m/z* 547.2293 $[M+H]^+$ (calcd for $C_{27}H_{35}N_2O_{10}$, 547.2286); ^1H and ^{13}C NMR data (CD_3OD, 500 and 125 MHz) see Tables 1 and 2

3-Epicorynanthine ***(6):*** pale-yellow solid; [α] −20 (*c* 0.1, MeOH); UV (MeOH) λ_{max} (log ε): 223 (4.1), 282 (3.5) nm; ECD (0.0009 M, MeOH) λ_{max} ($\Delta\varepsilon$) 217 (+8.60), 233 (−7.08), 273 (−3.30); IR (KBr) *v*max 3420, 2923, 2852, 1726, 1631, 1454, 1281, 1183 cm^{-1}; HRESIMS *m/z* 355.2013 $[M+H]^+$ (calcd for $C_{21}H_{27}N_2O_3$, 355.2016); ^1H and ^{13}C NMR data (CD_3OD, 500 and 125 MHz) see Tables 1 and 2

Uncarialine K ***(7):*** pale-yellow crystals; mp 240.2−241.8 °C; [α] 0 (*c* 0.1, MeOH); UV (MeOH) λ_{max} (log ε): 216 (4.4), 286 (3.9), 380 (3.5) nm; IR (KBr) *v*max 3446, 3374, 2952, 1725, 1669, 1494, 1276, 1216 cm^{-1}. HRESIMS *m/z* 389.1134 $[M+H]^+$ (calcd for $C_{22}H_{17}N_2O_5$, 389.1132); ^1H and ^{13}C NMR data (CD_3OD, 500 and 125 MHz) see Tables 1 and 2

Uncarialine L ***(8):*** yellow crystals; mp 281.2−282.6 °C; [α] 0 (*c* 0.1, MeOH); UV (MeOH) λ_{max} (log ε): 200 (3.8), 315 (3.4), 391 (3.3) nm; IR (KBr) *v*max 3432, 2920, 2851, 1736, 1616, 1365, 1111 cm^{-1}; HRESIMS *m/z* 345.1203 $[M+Na]^+$ (calcd for $C_{19}H_{18}N_2O_3Na$, 345.1210); ^1H and ^{13}C NMR data (CD_3OD, 500 and 125 MHz) see Tables 1 and 2

4.5. X-ray crystallographic analysis

Single crystals of compounds **7** and **8** were collected from MeOH at room temperature. Intensity data were collected on a Bruker ApexDuo diffractometer equipped with an Apex II CCD using Cu Kα radiation. Cell refinement and data reduction were performed with Bruker SAINT software. The structure was solved by direct methods using SHELXL-97. Refinements were performed with SHELXL-97 using full-matrix least-squares, with anisotropic displacement parameters for all the non-hydrogen atoms. The H atoms were placed in calculated positions and refined using a riding model. Molecular graphics were computed with PLATON.

Crystal Data of ***7***: $C_{22}H_{16}N_2O_5$, M = 388.37, a = 21.695(5) Å, b = 5.7758(16) Å, c = 29.426(12) Å, α = 90°, β = 90°, γ = 90°, V = 3687.(2) Å3, T = 150.(2) K, space group $Pna2_1$, Z = 8, μ(Cu Kα) = 0.836 mm^{-1}, 18820 reflections measured, 6022 independent reflections (R_{int} = 0.3162). The final R_1 values were 0.1737 ($I > 2\sigma(I)$). The final $wR(F^2)$ values were 0.4146 ($I > 2\sigma(I)$). The final R_1 values were 0.3545 (all data). The final $wR(F^2)$ values were 0.5170 (all data). The goodness of fit on F^2 was 1.229. Flack parameter = 0.2(10). Crystallographic data for **7** was sent to the CCDC with the number 2395497.

Crystal Data of ***8:*** $2(C_{19}H_{18}N_2O_3)\bullet 5(H_2O)$, M = 734.79, monoclinic, a = 14.1267(16) Å, b = 18.779(2) Å, c = 14.6205(15) Å, α = 90°, β = 109.903(5)°, γ = 90°, V = 3646.9(7) $Å^3$, Z = 4, T = 150(2) K, space group $P121/c_1$, μ(Cu Kα) = 0.821 mm^{-1}, 29140 reflections measured, 6648 independent reflections (R_{int} = 0.1084). The final R_1 value was 0.1471 ($I > 2\sigma(I)$), $wR(F^2)$ = 0.3939 ($I > 2\sigma(I)$). The final R_1 values were 0.1928 (all data). The final $wR(F^2)$ values were 0.4292 (all data). The goodness of fit on F^2 was 1.580. Crystallographic data for **8** was sent to the CCDC with the number 2395498.

4.6. Computational methods of ECD

For details, see the Supplementary Material.

4.7. In vitro α-glucosidase inhibition assay

As previously described with minor adjustments (Lu et al., 2024). In a 96-well microplate, 10 μL sample in PBS (0.1 M, pH 6.8) was mixed with 50 μL α-glucosidase solution (0.1 U/mL) and incubated for 15 min at 37 °C, 10 μL PBS was used as a blank control. Subsequently, 40 μL *p*NPG (5 mM) was added to the mixture as the substrate to initiate the reaction. After further incubation at 37 °C for 30 min, the reaction was terminated by adding 50 μL Na_2CO_3 (0.1 M). The absorbance was measured at 405 nm using a microplate reader.

4.8. α-Glucosidase enzyme kinetic assay

As previously described with minor adjustments (Lu et al., 2024). The kinetic analysis of compound **5** was measured using the reaction conditions in Section 4.5. Typically, three different concentrations of compound **5** around the IC_{50} value were chosen. Under each concentration, α-glucosidase activity was assayed by varying the concentration of *p*NPG as a substrate (Liu et al., 2013b). The inhibition type of active compound was determined by Lineweaver–Burk plots [the inverse of velocity ($1/v$) against the inverse of the substrate concentration ($1/[p\text{NPG}]$)] with substrate concentrations of 2.5, 5, 10, 20 μM. K_i and K_i' values were determined from $1/v$ versus [I] (Dixon plot) and S/v versus [I] plot, respectively.

4.9. Molecular docking of active compound 5 with α-glucosidase

The structure of α-glucosidase (3WY1) was obtained from the Protein Data Bank (PBD), and the 3D structures of the compound **5** was generated by Chem3D Pro 14.0. The water molecules of α-glucosidase were removed and all hydrogen atoms were added. The cubic grid box dimensions of α-glucosidase were defined as x = 86, y = 88, and z = 126 Å with spacing of 0.936 Å. Then, molecular docking was performed with Autodock Vina (Trott and Olson, 2010). Based on the minimum energy scoring, the best binding conformations between α-glucosidase and the candidates were selected from all docking results. Finally, the PyMOL molecular graphics system (version: 3.0.4) was used to visualize ligand-enzyme interactions.

CRediT authorship contribution statement

Kepu Huang: Writing – original draft, Methodology, Formal analysis. **Xuelin Chen:** Visualization, Methodology, Formal analysis. **Sheng Li:** Validation, Software, Data curation. **Xinjian Zhang:** Validation, Data curation. **Yumei Zhang:** Visualization, Software. **Yu Zhang:** Writing – review & editing, Supervision, Project administration, Funding acquisition, Conceptualization.

Declaration of competing interest

The authors declare the following financial interests/personal relationships which may be considered as potential competing interests: Yu Zhang reports financial support was provided by Yunnan Applied Basic Research Project. If there are other authors, they declare that they have no known competing financial interests or personal relationships that could have appeared to influence the work reported in this paper.

Acknowledgements

This work was financially supported by Yunnan Applied Basic Research Projects (202301AS070057), Strategic Priority Research Program of the Chinese Academy of Sciences (grant XDB1230000), National Key R&D Program of China (2022YFF1100301), Major Science and Technology Project of Henan Province (231100310200), Yunnan Province Science and Technology Department (202305AH340005).

Appendix A. Supplementary data

Supplementary data to this article can be found online at https://doi.org/10.1016/j.phytochem.2025.114490.

Data availability

Data will be made available on request.

References

Ali, E., Girl, V.S., Pakrashi, S.C., 1976. Vincarpine and dihydrovincarpine-two new zwitterionic indole alkaloids from *Vinca elegantissima* hort. Tetrahedron Lett. 17, 4887–4890. https://doi.org/10.1016/S0040-4039(00)78938-6.

Dong, Z.H., Pan, R.Y., Ren, G.Y., Zhou, M., Zhang, B., Fan, J.L., Qiu, Z.J., 2024. A novel antidiabetic peptide GPAGAP from *Andrias davidianus* collagen hydrolysates: screening, action mechanism prediction and improving insulin resistance in HepG2 cells. Food & Med. Homol 1, 9420010. https://doi.org/10.26599/FMH.2024.9420010.

Gul, S., Jan, F., Alam, A., Shakoor, A., Khan, A., AlAsmari, A.F., Alasmari, F., Khan, M., Bo, L., 2024. Synthesis, molecular docking and DFT analysis of novel *bis*-Schiff base derivatives with thiobarbituric acid for α-glucosidase inhibition assessment. Sci. Rep. 14, 3419. https://doi.org/10.1038/s41598-024-54021-z.

Hou, Z.W., Chen, C.H., Ke, J.P., Zhang, Y.Y., Qi, Y., Liu, S.Y., Yang, Z., Ning, J.M., Bao, G. H., 2021. α-Glucosidase inhibitory activities and the interaction mechanism of novel spiro-flavoalkaloids from YingDe green tea. J. Agric. Food Chem. 70, 136–148. https://doi.org/10.1021/acs.jafc.1c06106.

Huang, K.P., Xu, L.L., Li, S., Wei, Y.L., Yang, L., Hao, X.J., He, H.P., Zhang, Y., 2023. Uncarialines A-E, new alkaloids from *Uncaria rhynchophylla* and their anticoagulant activity. Nat. Prod. Bioprospect. 13, 13. https://doi.org/10.1007/s13659-023-00378-z.

Janot, M.M., Goutarel, R., Warnhoff, E.W., Le Hir, A., 1961. Stereoisomers of yohimbine. IV. New isomerizations and formation of 3-epicorynanthine and 3-epialloyohimbine. Bull. Soc. Chim. Fr. 637–644.

Kam, T.S., Lee, K.H., Goh, S.H., 1992. Alkaloid distribution in Malaysian *Uncaria*. Phytochemistry 31, 2031–2034. https://doi.org/10.1016/0031-9422(92)80356-J.

Khan, M., Ahad, G., Alam, A., Ullah, S., Khan, A., Salar, U., Wadood, A., Ajmal, A., Khan, K.M., Perveen, S., 2024. Synthesis of new bis (dimethylamino) benzophenone hydrazone for diabetic management: in-vitro and in-silico approach. Heliyon 10, e23323. https://doi.org/10.1016/j.heliyon.2023.e23323.

Li, N., Zhu, H.T., Wang, D., Zhang, M., Yang, C.R., Zhang, Y.J., 2020. New flavoalkaloids with potent α-glucosidase and acetylcholinesterase inhibitory activities from Yunnan black tea 'Jin-Ya'. J. Agric. Food Chem. 68, 7955–7963. https://doi.org/10.1021/acs.jafc.0c02401.

Liang, J.H., Luan, Z.L., Tian, X.G., Zhao, W.Y., Wang, Y.L., Sun, C.P., Huo, X.K., Deng, S., Zhang, B.J., Zhang, Z.J., Ma, X.C., 2019. Uncarialins A-I, monoterpenoid indole alkaloids from *Uncaria rhynchophylla* as natural agonists of the 5-HT_{1A} Receptor. J. Nat. Prod. 82, 3302–3310. https://doi.org/10.1021/acs.jnatprod.9b00532.

Liu, L., Li, S., Zhang, Q., Zhu, F., Yang, W., He, H., Hao, X., 2013a. Four new indole alkaloids from *Neolamarckia cadamba*. Chin. J. Chem. 31, 79–83. https://doi.org/10.1002/cjoc.201201016.

Liu, S.K., Hao, H., Bian, Y., Ge, Y.X., Lu, S., Xie, H.X., Wang, K.M., Tao, H., Yuan, C., Zhang, J., 2021a. Discovery of new α-glucosidase inhibitors: structure-based virtual screening and biological evaluation. Front. Chem. 9, 639279. https://doi.org/10.3389/fchem.2021.639279.

Liu, Y., Ma, L., Chen, W.H., Park, H., Ke, Z., Wang, B., 2013b. Binding mechanism and synergetic effects of xanthone derivatives as noncompetitive α-glucosidase inhibitors: a theoretical and experimental study. J. Phys. Chem. B 117, 13464–13471. https://doi.org/10.1021/jp4067235.

Liu, Y.P., Li, Y.J., Zhao, Y.Y., Guo, J.M., Liu, Y.Y., Wang, X.P., Shen, Z.Y., Qiang, L., Fu, Y. H., 2021b. Carbazole alkaloids from the fruits of *Clausena anisum-olens* with potential PTP1B and α-glucosidase inhibitory activities. Bioorg. Chem. 110, 104775. https://doi.org/10.1016/j.bioorg.2021.104775.

Lounasmaa, M., Hanhinen, P., 1999. Conformational study of geissoschizine isomers and their model compounds. Heterocycles 51, 649–670. https://doi.org/10.3987/rev-98-512.

Lu, J., Wang, H.L., Chen, X.L., Zhang, K., Zhao, X., Xiao, Y.X., Yang, F.X., Han, M., Yuan, W.Y., Guo, Y.L., Zhang, Y.M., 2024. Exploration of potential antidiabetic and antioxidant components from the branches of *Mitragyna diversifolia* and possible mechanism. Biomed. Pharmacother. 180, 117450. https://doi.org/10.1016/j.biopha.2024.117450.

Ong, K.L., Stafford, L.K., McLaughlin, S.A., Boyko, E.J., Vollset, S.E., Smith, A.E., Dalton, B.E., Duprey, J., Cruz, J.A., Hagins, H., 2023. Global, regional, and national burden of diabetes from 1990 to 2021, with projections of prevalence to 2050: a systematic analysis for the Global Burden of Disease Study 2021. Lancet 402, 203–234. https://doi.org/10.1016/S0140-6736(23)01301-6.

Qin, N., Lu, X., Liu, Y., Qiao, Y., Qu, W., Feng, F., Sun, H., 2021. Recent research progress of *Uncaria* spp. based on alkaloids: phytochemistry, pharmacology and structural

chemistry. Eur. J. Med. Chem. 210, 112960. https://doi.org/10.1016/j.ejmech.2020.112960.

Teerapongpisan, P., Suthiphasilp, V., Kumboonma, P., Maneerat, T., Duangyod, T., Charoensup, R., Promnart, P., Laphookhieo, S., 2024. Aporphine alkaloids and a naphthoquinone derivative from the leaves of *Phaeanthus lucidus* Oliv. and their α-glucosidase inhibitory activity. Phytochemistry 220, 114020. https://doi.org/10.1016/j.phytochem.2024.114020.

Trott, O., Olson, A.J., 2010. AutoDock Vina: improving the speed and accuracy of docking with a new scoring function, efficient optimization, and multithreading. J. Comput. Chem. 31, 455–461. https://doi.org/10.1002/jcc.21334.

Wenkert, E., Cochran, D.W., Hagaman, E.W., Schell, F., Neuss, N., Katner, A., Potier, P., Kan, C., Plat, M., 1973. Carbon-13 nuclear magnetic resonance spectroscopy of naturally occurring substances. XIX. Aspidosperma alkaloids. J. Am. Chem. Soc. 95, 4990–4995. https://doi.org/10.1021/ja00796a035.

Xu, X.T., Deng, X.Y., Chen, J., Liang, Q.M., Zhang, K., Li, D.L., Wu, P.P., Zheng, X., Zhou, R.P., Jiang, Z.Y., 2020. Synthesis and biological evaluation of coumarin derivatives as α-glucosidase inhibitors. Eur. J. Med. Chem. 189, 112013. https://doi.org/10.1016/j.ejmech.2019.112013.